PNAS RESEARCH ARTICLE | IMMUNOLOGY AND INFLAMMATION OPEN ACCESS

Visualizing the activation of encephalitogenic T cells in the ileal lamina propria by in vivo two-photon imaging

Isabel J. Bauer[a,1], Ping Fang[a,1], Katrin F. Lämmle[a], Sofia Tyystjärvi[b], Dominik Alterauge[c], Dirk Baumjohann[c,d], Hongsup Yoon[a,e,2], Thomas Korn[b,f], Hartmut Wekerle[a,e], and Naoto Kawakami[a,3]

Edited by Kenya Honda, Department of Microbiology and Immunology, Keio University School of Medicine, Tokyo, Japan; received February 18, 2023; accepted June 6, 2023 by Editorial Board Member Tadatsugu Taniguchi

Autoreactive encephalitogenic T cells exist in the healthy immune repertoire but need a trigger to induce CNS inflammation. The underlying mechanisms remain elusive, whereby microbiota were shown to be involved in the manifestation of CNS autoimmunity. Here, we used intravital imaging to explore how microbiota affect the T cells as trigger of CNS inflammation. Encephalitogenic CD4$^+$ T cells transduced with the calcium-sensing protein Twitch-2B showed calcium signaling with higher frequency than polyclonal T cells in the small intestinal lamina propria (LP) but not in Peyer's patches. Interestingly, nonencephalitogenic T cells specific for OVA and LCMV also showed calcium signaling in the LP, indicating a general stimulating effect of microbiota. The observed calcium signaling was microbiota and MHC class II dependent as it was significantly reduced in germfree animals and after administration of anti-MHC class II antibody, respectively. As a consequence of T cell stimulation in the small intestine, the encephalitogenic T cells start expressing Th17-axis genes. Finally, we show the migration of CD4$^+$ T cells from the small intestine into the CNS. In summary, our direct in vivo visualization revealed that microbiota induced T cell activation in the LP, which directed T cells to adopt a Th17-like phenotype as a trigger of CNS inflammation.

T cells | autoimmunity | central nervous system | intravital imaging | calcium signaling

Significance

Autoreactive T cells exist in the healthy immune repertoire but do not inherently induce CNS autoimmunity. It has been shown that the infiltration of these T cells can induce CNS inflammation, such as multiple sclerosis, yet the trigger for T cell infiltration remains elusive. In this study, we show that the autoreactive T cells do get stimulation from small intestinal microbiota which results in phenotypical changes of the T cells. The results indicate how and where preexisting autoreactive T cells get triggered to initiate immune reactions. The results open therapeutic avenues to prevent autoimmunity.

Multiple sclerosis (MS) is an autoimmune demyelinating disease of the central nervous system (CNS). MS is initiated and driven by autoreactive T cells, that preexist in the healthy repertoire (1). The T cells are primed in a peripheral site to penetrate the blood–brain barrier (BBB), infiltrate the CNS, and attack the local tissue. The site of immune cell activation and the activating mechanisms have remained undetermined. However, over the past years, an increasing body of evidence points to the intestinal tract that harbors trillions of microbial organisms which modulate local and systemic immune activity, including the activation of encephalitogenic T cells as described below.

Several observations support an active role of the intestine in the pathogenesis of MS. In fact, large-scale metagenomic trials associate particular gut microbial profiles with clinical MS (2). Furthermore, studies of rodent models of spontaneous experimental autoimmune encephalomyelitis (EAE) revealed that the development of MS-like CNS disease strictly depends on the presence of intact intestinal microbiota (3), with germfree (GF) animals being protected. Moreover, a follow-up study showed that human gut microbiota influence spontaneous EAE. The transplantation of fecal samples from monozygotic twins discordant for MS induced EAE with significantly higher incidence as compared to feces from the healthy twin (4). This microbiota-driven effect was supported by an independent study showing that also actively induced EAE is affected by the presence or absence of microbiota from MS patients vs. healthy controls (5). While these studies provided strong evidence of an active contribution of the gut microbiome to the triggering of CNS autoimmune disease, they did not directly illuminate the location and mechanisms of autoimmune activation within the gut-associated lymphoid tissue (GALT).

We here leveraged an advanced intravital imaging approach to visualize cellular function in vivo. The method does not only allow visualizing motility of immune cells in living tissue (6) but also their activation (7–9). We harnessed a recombinant calcium-sensing protein, Twitch-2B, to detect changes in intracellular calcium concentration indicating cellular activation. The sensor distinguishes short-lasting calcium signaling that is induced by, for example, chemokine signaling from antigen-dependent long-lasting calcium signaling, which is induced via MHC-TCR interaction. The combination of antigen-specific TCR transgenic mouse lines, a calcium-sensing protein, and two-photon intravital imaging constitutes a unique and reliable system to visualize and characterize the potential T cell stimulation in the small intestine of mice. In the present study, we took a closer look at

Author contributions: I.J.B., P.F., H.W., and N.K. designed research; I.J.B., P.F., K.F.L., and S.T. performed research; D.A., D.B., H.Y., and T.K. contributed new reagents/analytic tools; I.J.B., P.F., and K.F.L. analyzed data; and I.J.B., H.W., and N.K. wrote the paper.

The authors declare no competing interest.

This article is a PNAS Direct Submission. K.H. is a guest editor invited by the Editorial Board.

[1]I.J.B. and P.F. contributed equally to this work.

[2]Present address: School of Life Science, Handong University, Pohang, Gyeongbuk 37554, South Korea.

[3]To whom correspondence may be addressed. Email: Naoto.kawakami@med.uni-muenchen.de.

This article contains supporting information online at https://www.pnas.org/lookup/suppl/doi:10.1073/pnas.2302697120/-/DCSupplemental.

Published July 19, 2023.

the ileal lamina propria (LP) as the potential site of antigen-specific T cell stimulation.

Methods

Animals. C57BL/6J wild-type mice, TCR^{MOG} mice (also known as 2D2) (10), OT-II mice (11), SMARTA mice (12) and 2D2 × TH $PhAM^{T}$ mice (crossing $PhAM^{floxed}$ reporter mice (13), CD4-Cre mice (14) and 2D2 mice and BCRMOG mice (also known as TH) (15) were bred in the Core Facility Animal Models of the Biomedical Center, LMU Munich, or a specific pathogen-free (SPF) facility at the Technical University of Munich. 2D2 mice have been reported to develop spontaneous EAE in around 4% of cases; however, the rate at which mice get spontaneous EAE in our facility is 0%. The GF mice were bred in the animal facilities of the Technical University of Munich (School of Life Sciences Weihenstephan) and were kindly provided by Dirk Haller. The local authority (Regierung von Oberbayern) approved all mouse experiments.

Preparation of Single-Cell Suspensions and T Cell Culture. Lymph nodes and spleens were passed through a 40-μm cell strainer (Greiner Bio-One), followed by gravity centrifugation (400 *g*, 4 °C, 5 min). Blood was drawn from the heart into a syringe that had been flushed with heparin (5,000 U/mL) (Sigma-Aldrich) in PBS. Spleen and blood samples underwent erythrocyte lysis with ACK solution [NH_4Cl 8.024 mg/l (Merck), $KHCO_3$ 1.001 mg/l (Merck), and EDTA.$Na_2{\cdot}2H_2O$ 3.722 mg/l (Merck)].

For retroviral T cell transduction experiments, B cells from lymph nodes and spleens were first depleted from the cell suspensions using the Dynabeads B220 depletion kit (Thermo Fisher). The remaining T cells were then cultured in the presence of 0.5 μg/mL anti-CD3 (500A2, Invitrogen) and anti-CD28 (37.51, Invitrogen)-stimulating antibodies in complete DMEM (Sigma-Aldrich) [supplemented with 2 mM L-Glutamine (Sigma-Aldrich), 100 μg/mL Penicillin/Streptomycin (Sigma-Aldrich), 36 mg/l Asparagine (Sigma-Aldrich), 1 mM Sodium-Pyruvate (Sigma-Aldrich), 10 mL/l Nonessential amino acids (Sigma-Aldrich), 4 μL/l β-Mercaptoethanol (Merck KGaA), and 10% fetal calf serum (Sigma-Aldrich)] at a concentration of 2×10^6 cells/ml in a 12-well tissue culture plate (2 mL/well) for 2 d.

Retroviral Transduction of T Cells and Adoptive Transfer into Recipient Mice. For the generation of retrovirus harboring Twitch-2B DNA, HEK293T cells (American Type Culture Collection) were cultured in complete DMEM (see above) and transfected using the polyethylenimine (PEI max) (Polysciences) transfection method with 6 μg of pMSCV-Δneo-Twitch-2B and 3.5 μg of pCL-Eco plasmid. The culture medium was refreshed at 24 h after PEI transfection. The virus-containing supernatant was harvested after 48 h and 72 h, and viral particles were concentrated using Amicon® Ultra Filters (100-kDa cutoff, Merck).

After 2 d of culture, T cells were resuspended at a concentration of 4×10^6 cells/mL in complete DMEM with the concentrated retroviral supernatant at a dilution of 1:10, supplemented with 8 μg/mL polybrene (Sigma-Aldrich) and 10 ng/mL IL-2 (PeproTech). The T cells were spin-infected in 12-well plates with 0.5 mL per well (2,000 *g*, room temperature, 90 min). Typically, transduction yield was around 50%.

A total of 20 to 30×10^6 Twitch-2B transduced T cells were transferred intravenously into C57BL/6J wild-type SPF or GF mice 1 d after retroviral transduction.

Surgical Exposure of the Ileal LP. Prior to surgery, the mice were anesthetized with a cocktail of medetomidine, midazolam, and fentanyl [MMF; (5, 0.5, and 0.05 mg per kg body weight, respectively], tracheotomized, and ventilated with 1.5% isoflurane throughout the surgery and imaging procedure (16). Their body temperature was regulated using a custom-made heated microscope stage, and physiological parameters were constantly monitored during imaging. The blood vessels were visualized by i.v. infusion of Texas Red-conjugated dextran (50 μg, 70 kDa, Invitrogen). For one set of experiments, 100 μg of an anti-MHCII blocking antibody (clone M5/114.115.2, BioLegend) was injected (i.v.). During imaging, the abdomen was opened by midline incision. The ileum, more specifically close to the cecum, was taken out as little as necessary, and a PP-rich section was placed on a custom-made stage padded by dampened tissues. The intestinal tube was opened with a longitudinal incision of approximately 1 cm using a cautery pen (Bovie). Both sides were folded back onto the dampened tissues on the stage to have a flat layer exposing the ileal LP. The intestinal content was carefully removed before fixing the gut with a cover slip and tissue adhesive (3M Animal Care Products). The cover slip was pressed down so that peristaltic movements could not disturb image acquisition (17).

Photoconversion of T Cells in the Ileum. Photoconversion was performed as previously described (16) with some modifications. Briefly, asymptomatic 4-wk old 2D2 × TH $PhAM^{T}$ mice were anesthetized by i.p. injection of medetomidine (0.5 mg/kg), midazolam (5 mg/kg), and fentanyl (0.05 mg/kg). The fur was removed from the abdominal area using hair removal cream (Veet), and the body temperature was regulated by placing the mice on a custom-made heat mat. To expose the ileum, a 2-cm incision on the skin and the abdominal wall was made first. From the incision, the cecum, followed by the ileum, was pulled on a compression bandage soaked in 0.9% sodium chloride solution. T cells in the ileum were photoconverted from green to red fluorescence by irradiating the exposed ileum for 10 min with a 405-nm diode laser (LuxX 405-60, Soliton, OMI.115.15001). After the irradiation, buprenorphine (0.05 mg/kg) was given s.c. for analgesia, and the incisions were closed by sutures. The anesthesia was antagonized by i.p. injection of atipamezole (2 mg/kg), flumazenil (0.5 mg/kg), and naloxone (1.5 mg/kg). Mice were killed for analysis 3 d after the irradiation.

Surgical Exposure of the Ileal Peyer's Patches (PP). For imaging of the ileal PP, the same procedure as for the ileal LP imaging was applied with minor modifications. For the PP imaging, the intestinal tube was not opened, but instead, the PPs were imaged from the outside. Therefore, the ileum with a PP facing the top was placed on the custom-made stage padded by dampened tissues and fixed from the top with a cover slip.

Intravital Two-Photon Microscopy. Time-lapse two-photon laser-scanning microscopy was performed using a SP2 or SP8 MP microscope (Leica) as described previously (17). The SP2 system was equipped with a 10 W Millenia/Tsunami laser (Spectra Physics, Darmstadt, Germany). The excitation wavelength was tuned to 835 nm and routed through a water immersion objective (25×, NA 0.95, Leica). With a zoom factor of two, areas of 240 × 240 μm size were scanned, and 30- to 50-μm z-stacks were acquired with 3- to 4-μm z-step size. The acquisition rate was 25-s interval time with images line-averaged twice. Fluorescent signals were detected using nondescanned photomultiplier tube detectors equipped with 475/50-nm, 537/26-nm, 630/69-nm, and 685/40-nm bandpass filters (Semrock).

Multiphoton microscopy using the SP8 MP microscope was performed at the Core Facility Bioimaging of the Biomedical Center, LMU Munich. The SP8 system featured a pulsed InSight DS+ laser (Spectra Physics), and emission was tuned to 841 nm and routed through a water immersion objective (25×, NA 1.0, Leica). Using a 2× zoom, areas of 221 × 221 μm were scanned and acquired in 30- to 50-μm z-stacks with 3- to 4-μm step size and an acquisition rate of 25 s per z stack. Images were recorded with external, nondescanned hybrid photodetectors (HyDs) equipped with 483/32-nm, 535/30-nm, 585/40-nm, and 650/50-nm bandpass filters.

Image Processing and Analysis. Time-lapse images were acquired with Leica LCS software (Leica) for the SP2 system and with LAS X software (Leica) for the SP8 setup, respectively, and processed and analyzed using ImageJ (NIH, Bethesda, MD, USA) as described previously (17).

A Gaussian blur filter was used before Z-projecting the stacks with maximum intensity to generate two-dimensional movies. For Twitch-2B-transduced cells, ratiometric pseudocolor images were obtained by dividing the cpVenusCD (FRET) by the mCerulean3 (CFP) channel and changing to a fire lookup table. To analyze the calcium ratios, the cell shapes were manually outlined in each time frame in the 2D maximum projection to create a region of interest (ROI) for every cell to be tracked. The bleed-through of CFP into the YFP channel was determined to be 44%; hence, the FRET signal was corrected as YFP = FRET – 0.44 × CFP. The average signal intensities of all pixels in each ROI were defined to calculate the calcium ratio at every given time point.

Lymphatic Cannulation. In order to obtain efferent mesenteric lymphatic fluid and thus lymphocytes exiting the gut, the efferent mesenteric lymph duct was cannulated. Thirty min prior to cannulation, the animals were orally gavaged with 200 μL olive oil to visualize lymphatic vessels. The cannulation technique was modified from that of Druzd et al (18). In brief, the mice were anesthetized with MMF, and the skin was incised along the left costal arch, and the peritoneal cavity was opened. The efferent mesenteric lymphatic duct locates below the left

kidney. The cannulation tube [29G needle (BD) inserted into the tip of a 0.61-mm polyethylene tube (Warner Instruments)] was flushed with 15 µL heparin (5,000 U/mL). The cannulation tube was carefully inserted into the lymph duct, and the fluid was collected in a 29G syringe (BD). The liquid was washed with 10 ml PBS prior to flow cytometric staining.

Flow Cytometry and Cell Sorting. Cell suspensions from spleen, blood, and efferent mesenteric lymphatic fluid were stained with the following fluorochrome-conjugated antibodies: APC anti-mouse CD3 (clone 17A2, BioLegend, 1:200), FITC anti-mouse CD4 (RM4-5, BioLegend, 1:200), PE anti-mouse CD8 (53-6.7, BioLegend, 1:200), PerCP/Cy5.5 anti-mouse CD19 (6D5, BioLegend, 1:200). For dead cell exclusion, cells were stained with SYTOX™ Blue Dead Cell Stain (Invitrogen), and to avoid Fc-receptor binding, anti-mouse TruStain FcX (BioLegend) was used.

After the staining, $CD4^+$ T cells were sorted on a FACSAria IIIu (BD) using a 70-µm nozzle. Cell sorting was performed at the Core Facility Flow Cytometry of the Biomedical Center, LMU Munich. Flow cytometry data were analyzed using FlowJo (Tree Star Inc.).

For the analysis of photoconverted T cells, single-cell suspensions from the spleen and mononuclear cells from the CNS were prepared as previously described for flow cytometry (16). The following antibodies were used: APC anti-mouse CD62L (MEL-14, BD, 1:400), BV421 anti-mouse CD44 (IM7, BD, 1:400), and BV786 anti-mouse CD4 (RM4-5, BD, 1:800). Dead cells were detected with a near-infrared LIVE/DEAD dye (Thermo Fisher, 1:500), and nonspecific antibody binding to FC receptors was blocked with anti-mouse CD16/CD32 (2.4G2, BD; 1:200). The samples were acquired on a CytoFLEX flow cytometer (Beckman Coulter) and analyzed using FlowJo software (10.8.0).

Bulk-RNAseq. Total RNA was isolated from sorted $CD4^+$ T cells using the RNAeasy Plus microkit (Qiagen) as described previously (17). Quality and integrity of RNA was controlled on a Bioanalyzer 2100 (Agilent Technologies). Transcriptome analysis and subsequent bioinformatics were performed by BGI Group using their DNBseq™ platform. The sequence alignment to the reference genome was performed using HISAT2 (Hierarchical Indexing for Spliced Alignment of Transcripts two) (19). Differentially expressed genes (DEGs) were detected using DEseq2 (20).

Statistical Analysis. The statistical evaluation was performed using Prism software (GraphPad, San Diego, CA) as described in the figure legends. Significance was indicated by the *P*-value as follows: $*P < 0.05$, $**P < 0.01$, $***P < 0.001$.

Results

Calcium Signaling in TCR-Transgenic T Cells in the Ileal LP. We focused on the activation events taking place in the ileal wall containing microenvironments favoring immune cell activation. To calibrate calcium signaling in situ, we started out by imaging polyclonal $CD4^+$ T cells which were transduced to express the calcium indicator Twitch-2B at a high proportion prior to transfer into recipient mice (Fig. 1 *A* and *B*). Three days after transfer, Twitch-2B-labeled polyclonal $CD4^+$ T cells moved through the LP occasionally showing increased intracellular calcium (Fig. 1 *C–E* and Movie S1). We quantified the relative intracellular calcium levels (shown as the ratio of YFP/CFP) and instantaneous velocity at each time point of each cell (Fig. 1*C*). As observed previously

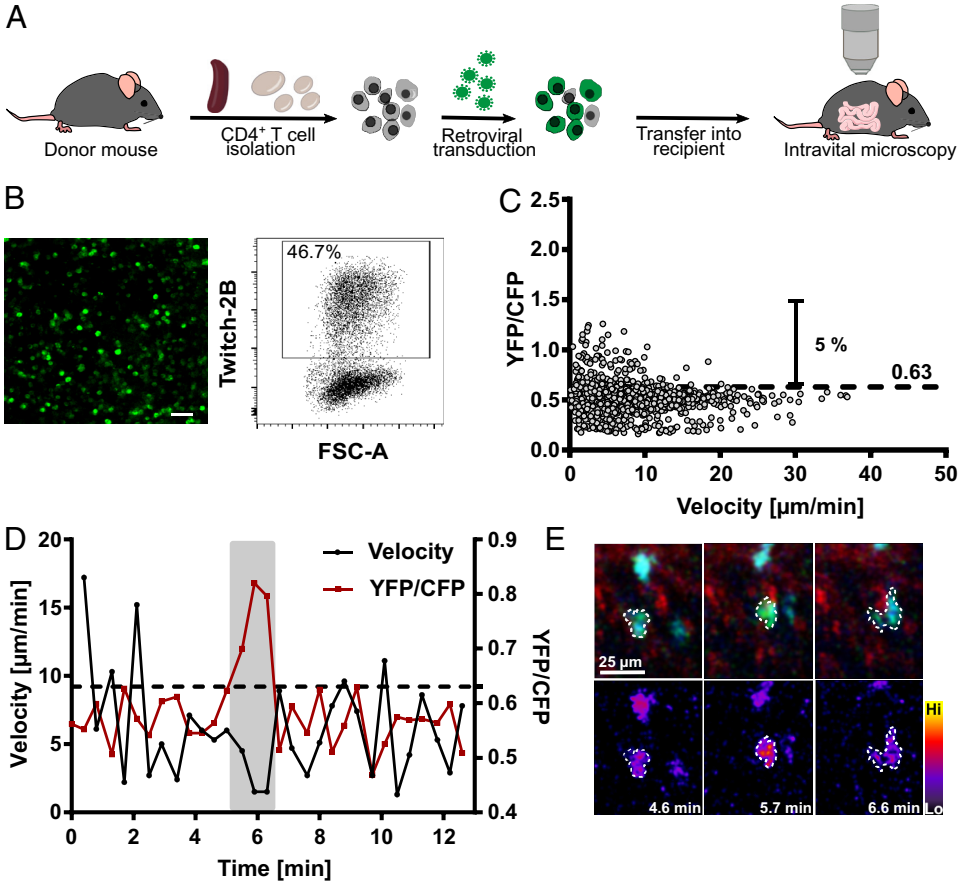

Fig. 1. Calcium ratio threshold definition using polyclonal T cells. (*A*) Schematic overview of the experimental design. (*B*) Polyclonal T cells on day 2 after transduction with a Twitch-2B containing retrovirus as seen in a fluorescence microscope and using flow cytometry. (*C*) Scatterplots showing polyclonal Twitch-$2B^+$ T cells' velocity versus calcium-indicator ratio change. The dotted line indicates the ratio threshold of YFP/CFP = 0.63. Each dot represents a single time point in a particular cell. Cumulative results encompass 3,306 FRET values of 109 cells from three independent experiments. (*D*) Representative track of a polyclonal T cell (depicted in *E* indicated with a white dotted line) shows velocity [µm/min] and ratio [YFP/CFP] in each time frame. The red dotted line indicates the ratio threshold, and the gray background indicates the time points where the T cell showed calcium signaling. (*E*) A fluorescence overlay of Twitch-$2B^+$ T cells (*E*, *Top*) and a pseudocolor calcium ratio image (*E*, *Bottom*) are shown. Images were acquired by two-photon microscopy.

in rat T cells (9), calcium signaling and cellular velocity were negatively correlated (Fig. 1*D*). The threshold to classify calcium ratios as calcium signaling was set to be above 95% of all calcium ratios identified in polyclonal T cells.

As the next step, we used our protocol to transduce MOG-specific encephalitogenic CD4$^+$ T cells from 2D2-transgenic mice. After retroviral gene transfer, Twitch-2B-expressing MOG-specific CD4$^+$ T cells were transferred into recipient mice for intravital imaging (Movie S2). In MOG-specific 2D2 CD4$^+$ T cells, the frequency of calcium signaling was significantly higher than in polyclonal T cells (Fig. 2 *A* and *B*) with a negative correlation with velocity similar as in polyclonal T cells (Fig. 1*C*). The increased calcium signaling coincided with a decrease in the average velocity per cell (6.4 μm/min in polyclonal vs 4.8 μm/min in MOG-specific CD4$^+$ T cells) (Fig. 2*C*). Not only the frequency but also the duration of calcium signaling was increased in MOG-specific vs. polyclonal T cells. Both the duration and frequency of long-term calcium signaling (longer than 2 min) were significantly increased in MOG-specific vs. polyclonal CD4$^+$ T cells with a maximum duration of 16.4 vs. 4.62 min and average duration of 1.5 vs. 0.86 min. Among the MOG-specific CD4$^+$ T cells, 23.5% exhibited long-term calcium signaling as compared to only 3.7% in polyclonal CD4$^+$ T cells (Fig. 2 *D* and *E*). In contrast, short-lasting signals (shorter than 2 min) were observed at similar rates in both polyclonal and MOG-specific T cells (Fig. 2 *D* and *E*).

In order to understand whether the stimulation of MOG-specific CD4$^+$ T cells was restricted to the LP or could also be detected in the PPs, we performed intravital microscopy of Twitch-2B-transduced CD4$^+$ T cells in those lymphoid follicles on the ileal surface. As in the LP, polyclonal CD4$^+$ T cells served to define the threshold in PPs. The timeline of intravital microscopy in PPs was the same as in the LP shown in Fig. 1*A*. Representative time-lapse pictures displayed the motility and calcium activities of polyclonal CD4$^+$ T cells in a PP (Fig. 3*A*). The analysis of the calcium ratios in the polyclonal CD4$^+$ T cells revealed that the background signal in the PPs was a bit higher than in the LP, so the threshold was set to 0.73 (95% of the calcium ratios were below that value) (Fig. 3*C*). The subsequent examination of MOG-specific 2D2 CD4$^+$ T cells failed to detect increased calcium levels with 5.8% above threshold (Fig. 3 *B* and *D*). In contrast to the stimulation in the ileal LP, the proportion of T cells with long-term calcium signaling in the PP was not changed significantly depending on the TCR specificity of the cells. Likewise, the fraction of cells with short-term high-calcium signaling was not significantly increased in MOG-specific 2D2 CD4$^+$ T cells over polyclonal CD4$^+$ T cells [40.4 ± 7.8% (T_{MOG} cells) vs. 34.2 ± 8.2% (polyclonal T cells)] (Fig. 3*E*). The longest calcium signaling lasted 20 min in a MOG-specific CD4$^+$ T cell and 13 min in a polyclonal CD4$^+$ T cell, and in both, most calcium signals were lasting less than 2 min (Fig. 3*F*).

In order to control for endogenous MOG or its mimes as activators of 2D2 CD4$^+$ T cells, two transgenic T cell lines responding to antigens distinct from MOG, OVA-specific CD4$^+$ T cells from OTII-transgenic mice and LCMV-specific CD4$^+$ T cells from SMARTA mice were used. Dietary contamination of OVA in the mouse chow and inadvertent infection with LCMV were ruled

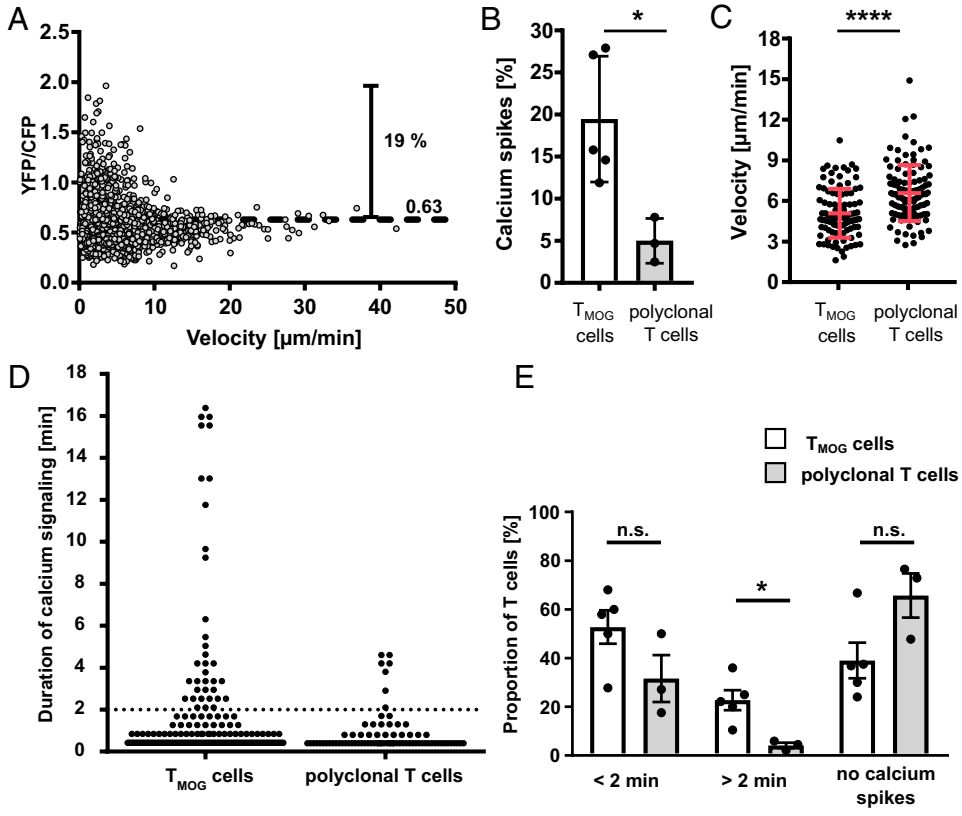

Fig. 2. Calcium signaling of MOG-specific T cells in the ileal LP. (*A*) Twitch-2B-labeled T cells were imaged in the ileal LP on day 3 p.t. Cumulative scatterplots showing velocity vs. calcium-indicator ratio change of MOG-specific Twitch-2B$^+$ T cells. The dotted line indicates the ratio threshold of YFP/CFP = 0.63. Each dot represents a single time point in a particular cell. Cumulative results encompass 4,001 FRET values of 98 cells from five independent experiments. (*B*) Relative amount of calcium signals above threshold. Each dot represents one independent experiment. (*C*) Average velocities of T cells in the ileal LP. Each dot represents one cell; the results are the sum of five (MOG-specific T cells) and three (polyclonal T cells) independent experiments. (*D*) Cumulative plots of high-calcium signaling of MOG-specific vs. polyclonal T cells in the ileal LP. The dotted line at 2 min indicates the cutoff between short-term and long-term calcium signaling. (*E*) Relative amounts of T cells with short-term (< 2 min), long-term (> 2 min), or no calcium signaling. (*B*, *C*, and *E*) The two-tailed *t* test is applied for statistical evaluation.

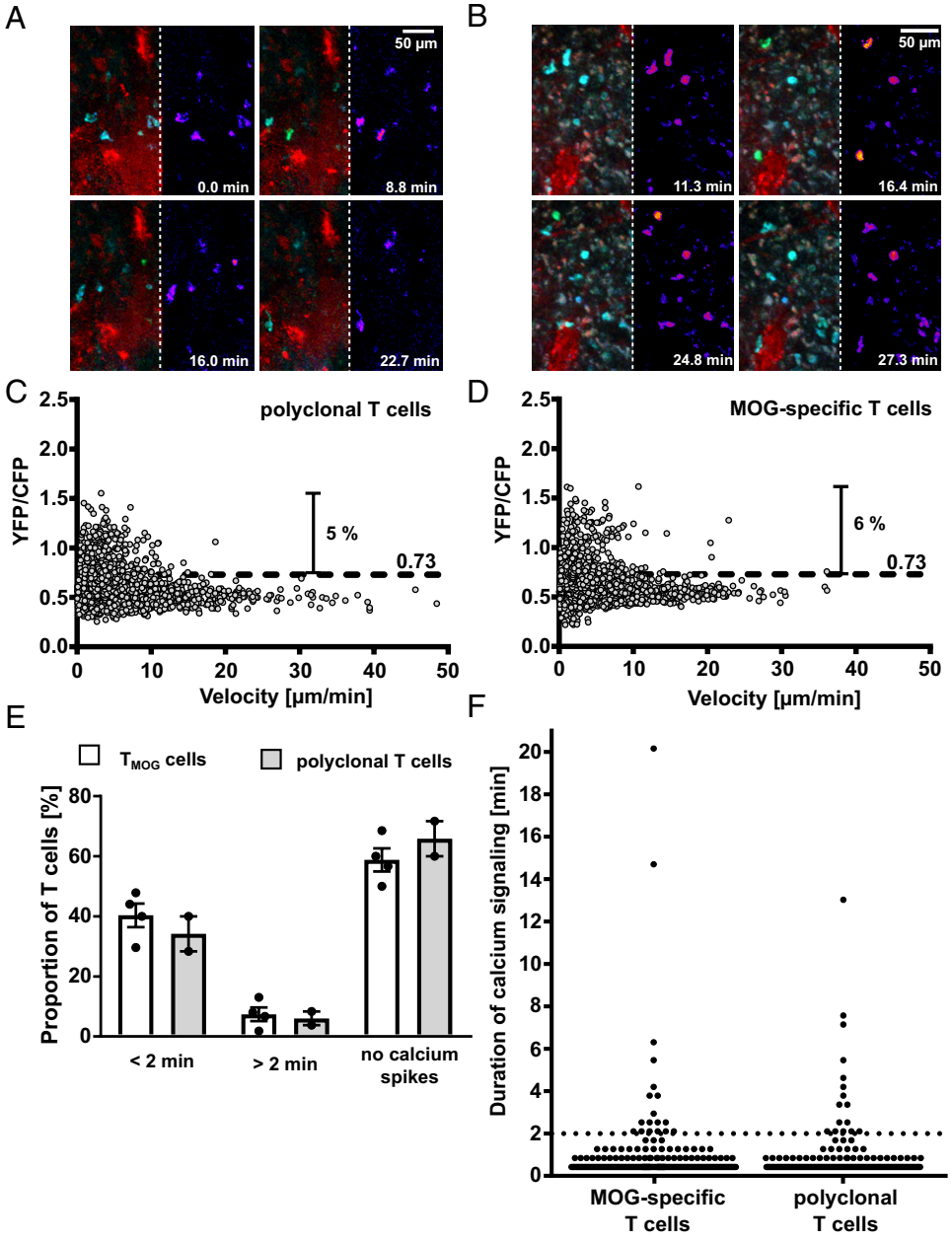

Fig. 3. Calcium signaling of polyclonal and MOG-specific T cells in the Peyer's patches. (*A* and *B*) A fluorescence overlay of Twitch-2B+ polyclonal (*A*) or MOG-specific (*B*) T cells (*Left*) and a pseudocolor calcium ratio image (*Right*) are shown. Images were acquired by two-photon microscopy. (*C* and *D*) Scatterplots showing polyclonal (*C*) and MOG-specific (*D*) Twitch-2B$^+$ T cells' velocity versus calcium-indicator ratio change. The dotted line indicates the ratio threshold of YFP/CFP = 0.73. Each dot represents a single time point in a particular cell. Cumulative results encompass 7,704 (T_{MOG} cells) and 7,195 (polyclonal) FRET values of 155 (T_{MOG} cells) or 140 (polyclonal) cells from three or two independent experiments, respectively. (*E*) Relative amounts of MOG-specific or polyclonal T cells exhibiting short-term (< 2 min), long-term (> 2 min), or no calcium signaling. (*F*) Cumulative plots indicating the duration of the individual high-calcium spikes of MOG-specific vs. polyclonal T cells in the PPs. The dotted line at 2 min indicates the cutoff between short-term and long-term calcium signaling.

out. Unexpectedly, OTII CD4$^+$ T cells showed similar calcium activities as 2D2 CD4$^+$ T cells (Fig. 4 *A* and *C* and Movie S3). Also, SMARTA CD4$^+$ T cells showed an increased amount of calcium signals above threshold similar to 2D2 and OTII CD4$^+$ T cells (Fig. 4 *B* and *D*). The maximum durations of the calcium spikes were 13 and 8.4 min for OVA-specific CD4$^+$ T cells and LCMV-specific CD4$^+$ T cells, respectively, with an average duration of 1.2 min in OVA- and 1.1 min in LCMV-specific CD4$^+$ T cells (Fig. 4*E*). The proportion of T cells exhibiting long-term calcium signaling was increased in all TCR-transgenic T cells as compared to polyclonal CD4$^+$ T cells, whereby the increase was less pronounced in the LCMV-specific CD4$^+$ T cells [4.2 ± 1.9% (polyclonal) vs. 22.8 ± 9.2% (MOG) vs. 26 ± 17.2% (OVA) vs. 12.7 ± 2.2% (LCMV)]. Not only the long-term spikes but also the proportion of T cells with short-term calcium signaling was higher in the TCR-transgenic cells: 31.6% of polyclonal CD4$^+$ T cells exhibited short-lasting high-calcium signals in contrast to 52.7% in MOG-specific CD4$^+$ T cells, 63.6% in OVA-specific CD4$^+$ T cells and 58.3% in LCMV-specific CD4$^+$ T cells (Fig. 4*F*).

Mechanisms to Induce Calcium Signaling in T Cells. MOG TCR–transgenic mice develop spontaneous EAE under SPF but not under GF conditions, indicating that the encephalitogenic T cells are activated via microbiota or derived factors from them (3). To test this, we transferred Twitch-2B-expressing 2D2 CD4$^+$ T cells into GF C57BL/6J mice. In the GF ileal LP of recipient mice,

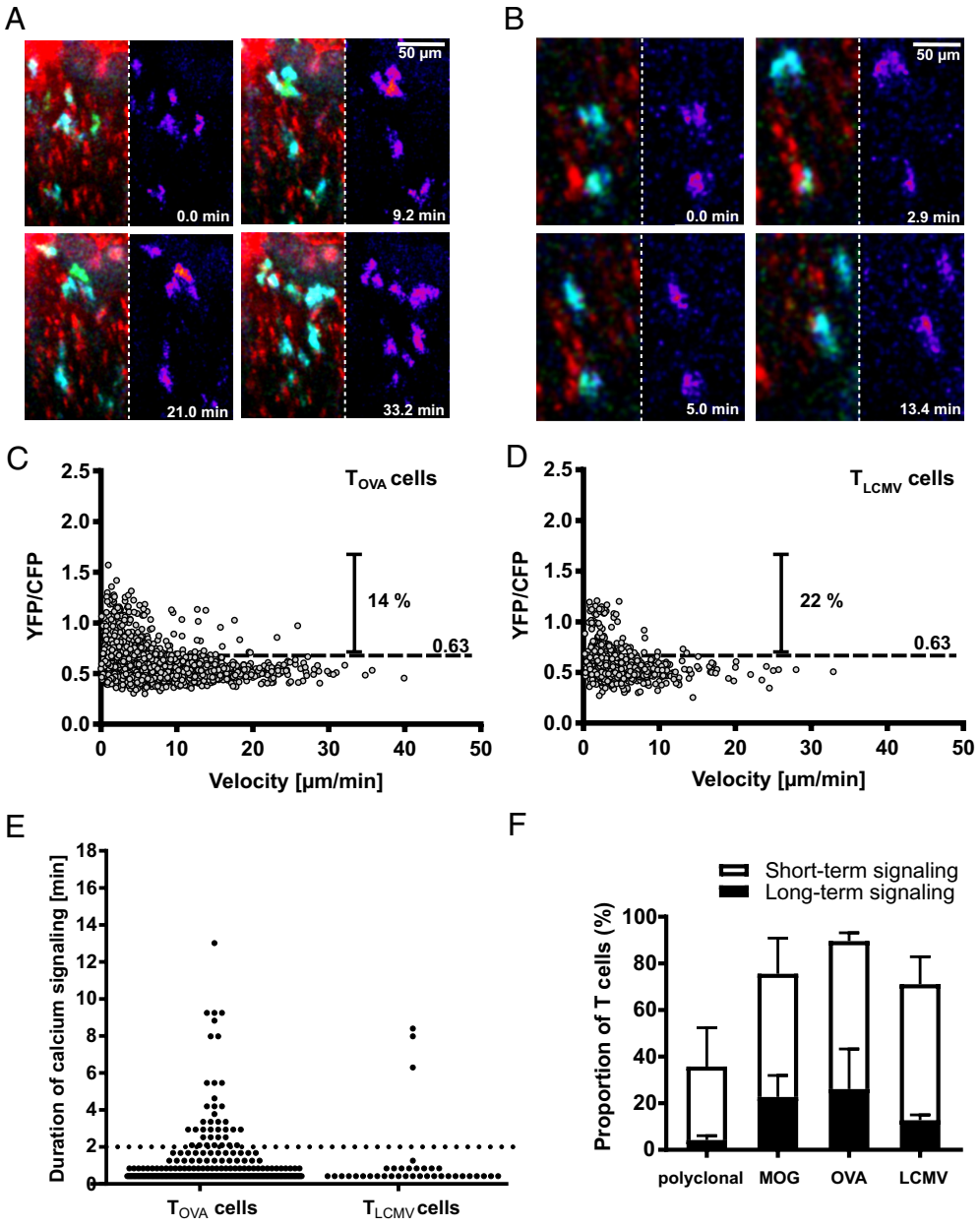

Fig. 4. Calcium signaling of OVA- and LCMV-specific T cells in the ileal LP. (*A* and *B*) A fluorescence overlay of Twitch-2B$^+$ OVA-specific (*A*) or LCMV- specific (*B*) T cells (*Left*) and a pseudocolor calcium ratio image (*Right*) are shown. Images were acquired by two-photon microscopy. (*C* and *D*) Scatterplots showing OVA-specific (*C*) and LCMV-specific (*D*) Twitch-2B$^+$ T cells' velocity versus calcium-indicator ratio change. The dotted line indicates the ratio threshold of YFP/CFP = 0.63. Each dot represents a single time point in a particular cell. Cumulative results encompass 5,018 (OVA) or 736 (LCMV) FRET values of 125 (OVA) or 23 (LCMV) cells from three or two independent experiments, respectively. (*E*) Cumulative plots indicating the duration of the individual high-calcium spikes of OVA-specific vs. LCMV-specific T cells in the ileal LP. The dotted line at 2 min indicates the cutoff between short-term and long-term calcium signaling. (*F*) Summary of relative amounts of short-term (< 2 min) or long-term (> 2 min) calcium signaling in T cells with different TCR specificities.

the proportion of calcium ratios above threshold was drastically reduced in MOG-specific CD4$^+$ T cells as compared to the LP of recipients housed under SPF conditions (Fig. 5*A* and Movie S4). The vast majority of T cells (70.5 ± 5.4%) traveled through the GF ileal LP spontaneously without showing any calcium activities (Fig. 5*C*). Occasional short-term calcium signals were observed in the rest of the MOG-specific CD4$^+$ T cells (29.5 ± 5.4%), whereas long-term calcium signaling was completely missing in the absence of gut microbiota (Fig. 5 *B* and *C*). These results indicate that microbiota play a pivotal role in the induction of calcium signaling and hence activation of T cells in the ileal LP.

These experiments were complemented by applying anti-MHC class II blocking antibodies i.v. during intravital imaging. As shown in Fig. 5*D*, the intravenous injection of anti-MHC class II antibodies diminished calcium signaling in MOG-specific CD4$^+$ T cells significantly. The blocking antibody reduced the maximum time of calcium signaling from 18 min to 2.5 min (Fig. 5*E*), led to a decrease in the frequency of short-term calcium signaling, and subsequently suppressed long-term calcium signaling (Fig. 5*F*).

We next evaluated the effect of exogenous antigens. Twitch-2B-transduced OVA-specific CD4$^+$ OT-II T cells were adoptively transferred 3 d prior to microscopy along with an oral bolus of 4 mg OVA protein together with Texas-red conjugated 70-kDa dextran shortly before starting intravital microscopy. The fraction of elevated calcium ratios rose significantly over the calcium ratios of OVA-specific CD4$^+$ T cells without the exogenously applied antigen (Fig. 6*A*, compare Fig. 4*A*) (22% with vs. 14%

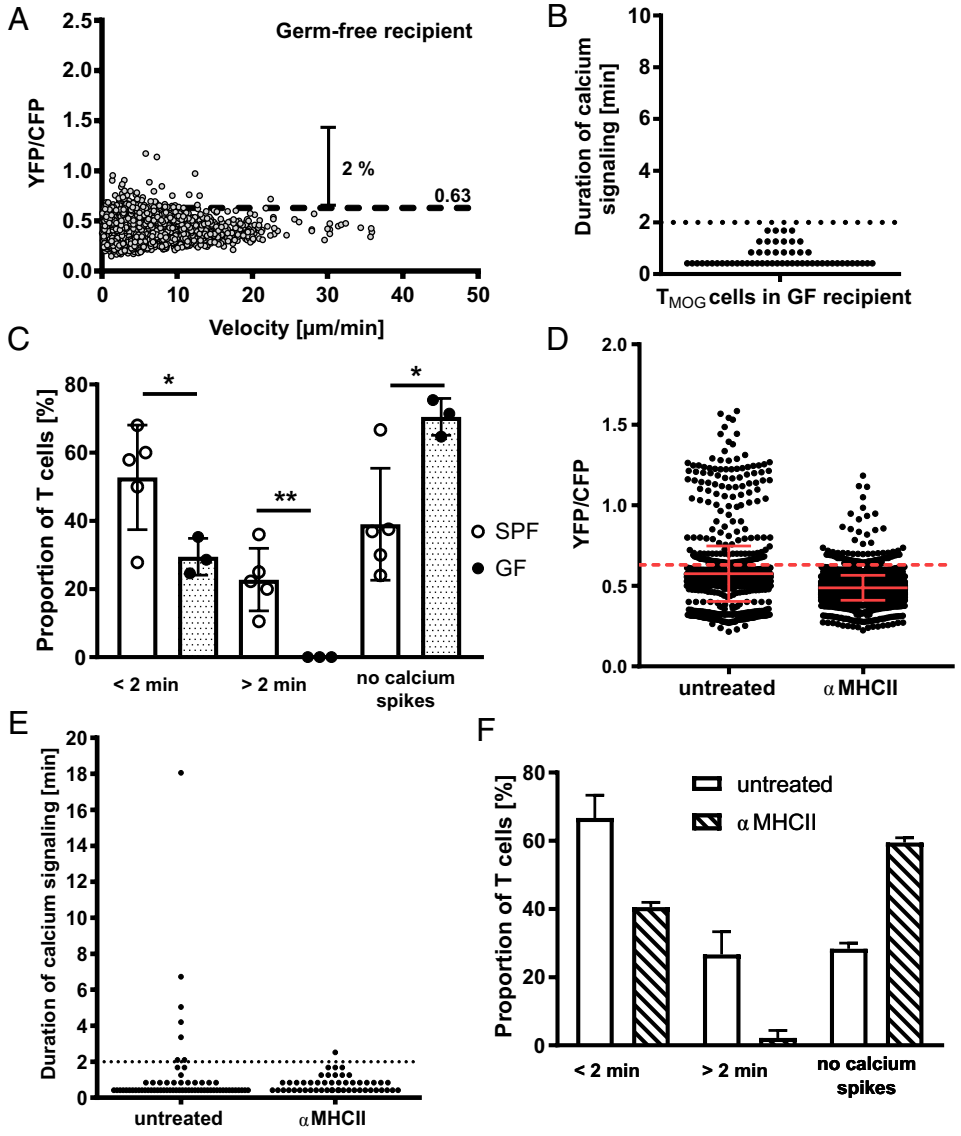

Fig. 5. Calcium signaling of T cells in the ileal LP of GF mice or after blocking of MHCII complexes. (*A*) Twitch-2B-labeled T cells were imaged in the ileal LP of mice housed under GF conditions. Cumulative scatterplots showing velocity vs. calcium-indicator ratio change of MOG-specific Twitch-2B$^+$ T cells. The dotted line indicates the ratio threshold of YFP/CFP = 0.63. Each dot represents a single time point in a particular cell. Cumulative results encompass 4,232 FRET values of 85 T cells from three independent experiments. (*B*) Cumulative plots indicating the duration of the individual high-calcium spikes MOG-specific T cells in the ileal LP of GF mice. The dotted line at 2 min indicates the cutoff between short-term and long-term calcium signaling. (*C*) Proportion of T cells with short-term (< 2 min), long-term (> 2 min), or no calcium signaling of MOG-specific T cells in the ileal LP of SPF vs. GF recipients. The two-tailed *t* test is applied for statistical evaluation. (*D*) Cumulative plots of the calcium ratio (YFP/CFP) before and after application of an anti-MHCII blocking antibody are shown. Each dot represents a single time point in a particular cell. (*E*) Cumulative plots indicating the duration of the individual high-calcium spikes of MOG-specific T cells in the ileal LP before and after application of anti-MHCII blocking antibody. The dotted line at 2 min indicates the cutoff between short-term and long-term calcium signaling. (*F*) Proportion of T cells with short-term (< 2 min), long-term (> 2 min), or no calcium signaling of MOG-specific T cells in the ileal LP before and after i.v. injection of an anti-MHCII blocking antibody. Results from three (*A*–*C*) or two (*D*–*F*) independent experiments.

without antigen). The intense red fluorescent signal indicated the penetration of orally applied antigen into the ileal LP at the time of microscopy (Fig. 6*B*). Interestingly, the calcium response of the stimulated CD4$^+$ T cells was time dependent: Most of the calcium signaling in the early phase was long lasting and then decreased over time to be replaced after 77 min completely by short-lasting calcium signaling. This suggests that the exogenous OVA entered the small intestine quickly and was promptly processed to transiently enhance T cell stimulation (Fig. 6*C*).

Migration and Transcriptome Analysis of GALT-Emigrating T Cells. Calcium signaling triggers phenotypical changes in T cells. These should be demonstrable in CD4$^+$ T cells emigrating from GALT. To this end, the efferent lymphatic vessels were cannulated, and lymphocytes were collected from the lymphatic fluid (18). The numbers of lymphocytes recovered from the GALT efferent lymphatic vessels differed depending on the mouse housing condition and genetic background (Fig. 7*A*). The highest counts were noted in the lymphatic fluid from mice housed under SPF conditions; among these, wild-type mice yielded a higher cell concentration (477 ± 313 cells/µL) than mice with a MOG-specific TCR transgene (237 ± 109 cells/µL). GF mice of either genetic background provided lymphatic fluid with further reduced cell numbers [205 ± 330 cells/µL (wild-type (wt) mice) and 101 ± 102 cells/µL (GF mice with MOG TCR)].

In the efferent mesenteric lymphatic fluid of wt mice, CD4$^+$ T cells constituted the predominant lymphocyte subset independent of the animals' hygiene condition [47% (SPF) vs. 48% (GF)]. In

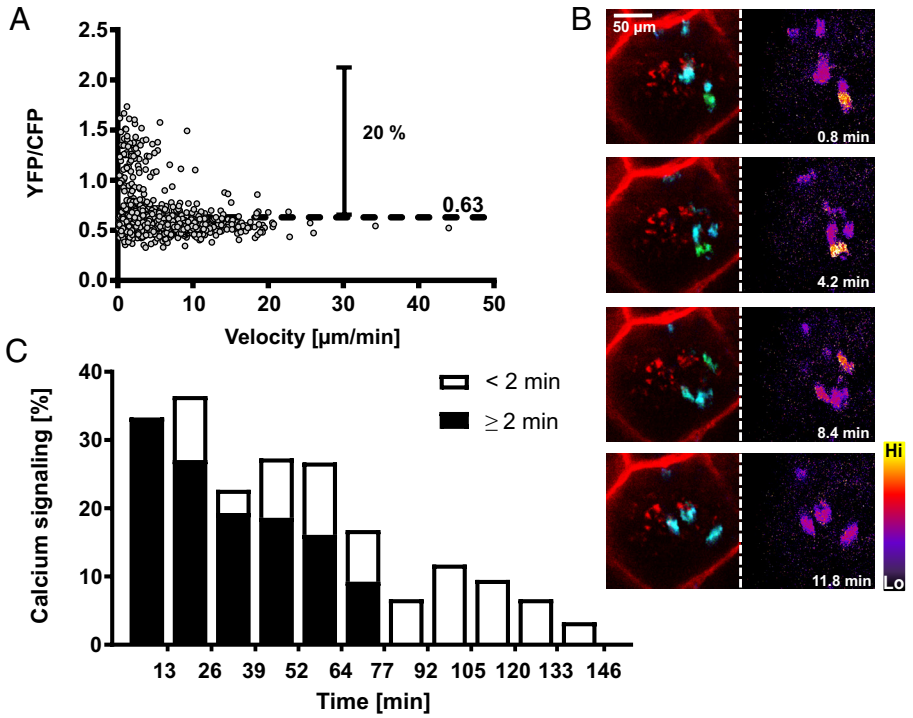

Fig. 6. Calcium signaling of T cells in the ileal LP after oral gavage of antigen. (*A*) Twitch-2B-labeled OVA-specific T cells were imaged in the ileal LP of mice that had been orally gavaged with OVA protein prior to imaging. Scatterplot showing velocity vs. calcium-indicator ratio change of OVA-specific Twitch-2B$^+$ T cells after oral gavage of OVA. The dotted line indicates the ratio threshold of YFP/CFP = 0.63. Each dot represents a single time point in a particular cell. Shown are 1,601 FRET values of 42 T cells. (*B*) A fluorescence overlay of Twitch-2B$^+$ OVA-specific T cells (*Left*) and a pseudocolor calcium ratio image (*Right*) are shown. Images were acquired by two-photon microscopy. (*C*) Proportion of calcium ratios associated with short-term (<2 min) or long-term (>2 min) calcium signaling over time in minutes from the onset of intravital imaging. Representative result from two independent experiments.

MOG TCR–transgenic mice, the CD4$^+$ population was increased to 66% and 51% in SPF and GF mice, respectively. In contrast, CD8$^+$ T cells, which were almost absent in the mesenteric lymphatic fluid [2% (SPF), 0.1% (GF)], which is probably due to the genetic modification by TCR transgene (10) (Fig. 7*B*).

By taking advantage of a photoconvertible protein, we tracked the migration of MOG-specific CD4$^+$ T cells from the ileal LP. Three days after photoconversion in the ileum, around 4% of CD4$^+$ T cells in the CNS harbored the photoconverted protein (Fig. 7*C*), suggesting that these T cells had freshly migrated to the CNS from the ileum. Further phenotypical analysis of the T cells showed that the photoconverted T cells in the CNS contained more antigen-experienced T cells (CD44^{high}, CD62L^{low}) than naive T cells, whereas the photoconverted T cells in the spleen contained more naive T cells (CD44^{low}, CD62L^{high}) than antigen-experienced T cells (Fig. 7*D*). These results indicate that antigen-experienced T cells migrated from the ileum into the CNS prior to clinical EAE.

CD4$^+$ T cells were sorted from lymphatic fluid, spleen, and blood as shown in the representative flow cytometry plots in *SI Appendix*, Fig. S1*A*, and bulk RNAseq was performed. The cluster dendrogram in *SI Appendix*, Fig. S1*B* shows that the MOG-specific CD4$^+$ T cells have specific transcriptome profiles dependent on the tissue compartment and hygiene conditions as expected. The impact of the housing condition appeared to be bigger than the one depending on the location since most of samples from SPF and GF clustered separately (*SI Appendix*, Fig. S1*B*). A volcano plot shows DEGs in MOG-specific T cells between SPF and GF recipients (Fig. 7*C*). To get a deeper insight into the role of the gut microbiota, the comparison between MOG-specific 2D2 T cells collected from lymphatic fluid and the spleen in SPF mice was included in the analysis in addition to the housing conditions (Fig. 7*D*). Among the up-regulated genes in the lymphatic fluid of SPF recipients, six genes (*Il22*, *Ccr6*, *Ahrr*, *Il17re*, *Il1r1*, and *Il23r*) were related to Th17 cells, which are considered a key player to induce CNS inflammation. Flow cytometric analysis confirmed an increased number of Th17 cells in 2D2 mice compared to wild-type mice, whereas the numbers of Th1 cells were similar (Fig. 7*G*). In addition, some genes, which are known to be involved in lymphocyte migration, were up regulated. For example, *Ccr6* encodes a receptor for CCL20 and is involved in T cell migration into the CNS (21). *Fndc7* and Lrfn encode fibronectins. Wagner et al. showed that fibronectin is up-regulated on the surface of activated T cells and plays a role in the proliferative capacity of those T cells (22). Although the numbers of DEG are limited, the results suggest that the MOG-specific T cells in SPF mice, where they show a higher rate of calcium signaling, tend to have increased numbers of Th17 cells. In contrast, the transcriptome analysis of polyclonal T cells from the efferent mesenteric lymphatic fluid from SPF vs. GF mice did not reveal differential gene expression in genes related to immune functions, which is in line with the absence of increased calcium signaling in polyclonal T cells (*SI Appendix*, Fig. S1*C*).

Discussion

We used the calcium-sensing protein Twitch-2B in combination with intravital two-photon microscopy to show that antigen-specific CD4$^+$ T cells receive stimulation from microbiota in the ileal LP. In addition, transcriptome analysis of GALT-emigrating T cells revealed that they are directed toward the Th17 axis, thus implicating them in the induction of inflammatory CNS disease.

It is well known that the small intestine is a major location for the peripheral induction of Th17 cells (23–25), which are essential

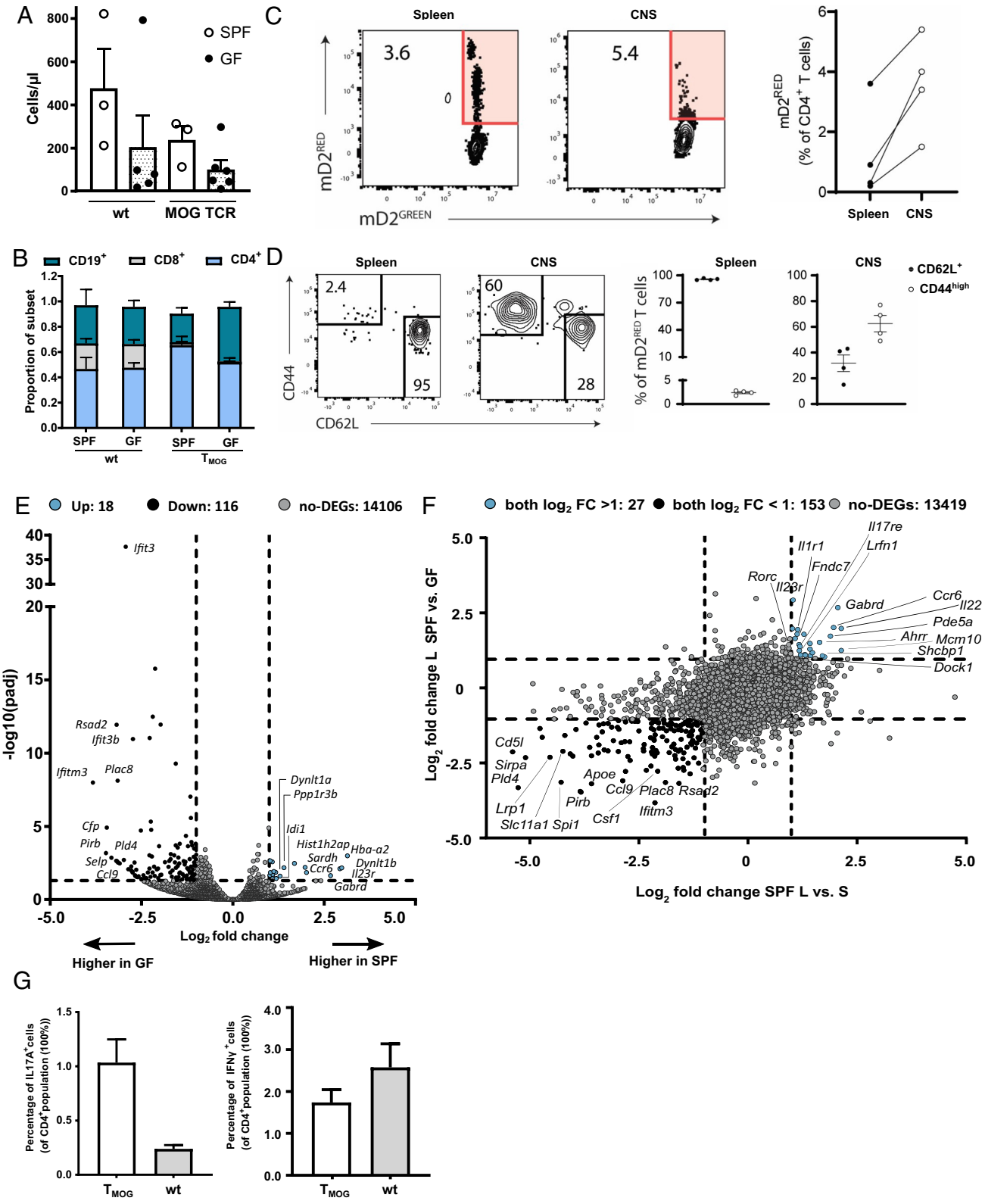

Fig. 7. Transcriptome analysis of GALT-emigrating T cells. Lymphocytes were isolated from the efferent mesenteric lymphatic fluid of wild-type and TCR transgenic mice housed under SPF or GF conditions, respectively. (*A*) Lymphocyte counts from the efferent mesenteric lymphatic fluid of different mouse lines housed under either SPF or GF conditions. (*B*) Relative amounts of $CD4^+$, $CD8^+$, and $CD19^+$ cells in the cannulated lymphatic fluid in the different mouse lines. (*C* and *D*) The percentage (*C*) and phenotype (*D*) of photoconverted T cells ($mD2^{RED}$) in the spleen and CNS on day 3 after photoconversion. The cells were pregated on $CD4^+$ and photoconvertible protein ($mD2^{GREEN}$) for *C* or photoconverted protein ($mD2^{RED}$) for *D*. Representative flow cytometry plots (*Left*) and summary (*Right* graph) are shown. n = 4 mice. (*E*) Volcano plot of DEGs from the transcriptomes of MOG-specific $CD4^+$ T cells from the efferent mesenteric lymphatic fluid of SPF (n = 3) vs. GF (n = 3) mice. The vertical dotted lines indicate the fold change cutoff of two, and the horizontal dotted line shows the adjusted *P*-value cutoff of 0.05. (*F*) Scatterplot of DEGs from SPF efferent mesenteric lymphatic fluid vs. spleen plotted against the DEGs from efferent mesenteric lymphatic fluid of mice housed under SPF vs. GF conditions. Dotted lines indicate the fold change cutoff of two. (*G*) Percentage of IL17A (*G*, *Left*) and IFNγ (*G*, *Right*) producing cells among all $CD4^+$ T cells in the efferent mesenteric lymphatic fluid from GALT are shown. Mean ± SD of five (T_{MOG}) and seven (wt) mice.

to maintain mucosal barrier functions (26) against extracellular pathogens (27) in a healthy status. In addition, Th17 cells promote autoimmunity in multiple organs including skin, lung, and intestine (28, 29) and CNS where Th17 cells are the key player in MS pathogenesis (30). Among microbiota, segmented filamentous bacteria have been shown to be sufficient to induce Th17 cells (31–33). However, it remained unclear how the stimulated T cells in the LP contribute to the pathogenesis.

Recently, Schnell et al. elegantly showed the presence of a homeostatic, stem-like T cell population which immigrates from peripheral lymphatic tissues into the intestine where it is maintained by the microbiota (34). Our present observations support and expand this concept by identifying (auto)antigen-specific T cells homing to specific GALT tissues and interacting there with local stroma cells. The T cells responded by elevated levels of intracellular calcium, depending on microbiota and MHC class II. These interactions happened within the ileal segment of the GALT, which is presumed to predominantly harbor proinflammatory processes, in contrast to the colon with its regulatory milieus. Although further studies are needed, the observed T cell stimulation is likely for maintaining stem-like Th17 cells, which can further differentiate into pathogenic Th17 cells.

T cell calcium responses came in two modes, distinguishable by their duration. A proportion of immigrant 2D2 T cells emitted short-lasting calcium signals, both in the LP as well as in the PPs. This response seems to be independent of specific antigen presentation but may contribute to the tonus of T cells (35) or contribute to their education similar to the autoantigen-specific T cells in the spleen (9, 36). In stark contrast, a 10 to 20% of antigen-specific T cells, including MOG-specific T cells, showed long-term calcium signaling in the ileal LP (Fig. 4*F*). This proportion is significantly higher than the one of T cells in the spleen, where they rarely showed calcium signaling (9). Long-term calcium signaling indicates productive recognition of specific antigen, which raises the question on the stimulating structure(s) within the LP. Besides in the CNS, myelin antigen-specific T cells can be stimulated by peripheral in neural structures (37), in AIRE expressing mimetic cells (38), or the autoantigens can be imported with diet. Alternatively, molecular mimicry of microbiota-derived antigens may stimulate the T cells in GALT.

Indeed, antigenic mimicry of MOG-specific 2D2 cells was shown in the case of cross-reaction to neurofilament-M (NF-M) (39). Comparable mechanisms could occur in the ileum with microbial mimotopes, with the key example here of Lactobacillus reuteri peptides and murine MOG-specific $CD4^+$ T cells (40).

Three findings could support intestinal mimicry. First, long-acting calcium responses critically depended on the presence of intact gut microbiota; they were absent in GF mice. Second, these responses were substantially reduced by mAbs blindfolding peptide-presenting MHC class II determinants, pointing to the function of TCR as receivers of antigenic signals. Third, orally introduced antigen increased the frequency of the long-acting responses from 14% (Fig. 4*C*) to >30% (Fig. 6*C*). This suggests that in the unfed animal, the antigen-presenting cells were not saturated by intrinsic (microbe-derived) antigen. The frequency of calcium signaling was the highest at the start of imaging, i.e., 40 min after gavage. The proportion of T cells with long-term calcium signaling gradually declined during imaging. Later, we observed only short-term calcium signaling, which can be explained as saturation of calcium signaling caused by excessive stimulation.

It is important to note, however, that the response pattern described was by no way unique to MOG-specific 2D2 cells. Ovalbumin-specific OT-II and LCMV-reactive $CD4^+$ T cells behaved very much the same way. Further studies are needed to answer whether the trillions of gut bacteria provide a universe of distinct mimotopes sufficient to activate a large proportion if not all (auto)antigen-specific T cells entering the GALT.

Another important factor to be considered is the affinity of TCRs, which can influence antigen recognition and the following intracellular calcium in the T cells. Transgenic TCRs, including 2D2, OTII and SMARTA, have higher affinity because they are selected from antigen-experienced T cells. Such high-affinity TCR may recognize antigen or MHC class II, which is usually not sufficient to induce T cell activation. However, this seems not to be the case in our observation. Although the SMARTA TCR has a >10,000-fold higher affinity to antigen than 2D2 (41), we observed comparable frequencies of calcium signaling in 2D2 T cells and in SMARTA T cells (Fig. 4*F*). Of note, to provide the same experimental setting for different transgenic T cells, all T cells used in this manuscript were stimulated with anti-CD3 and anti-CD28 antibodies followed by transduction with Twitch-2B-coding retrovirus before injection into recipient mice. Antigen stimulation was avoided since this may provide different degrees of stimulation in each transgenic T cell. It is worthwhile to mention that the stimulation observed in transgenic T cells is not mediated by coexpressed endogenous TCR. Hurst et al. showed that endogenous TCR, which can be coexpressed with transgenic TCR, may induce T cell activation (42). In our study, polyclonal T cells show occasional calcium activities in the ileal LP (Fig. 1*C*), which can be only induced via endogenous TCR as they do not harbor transgenic TCRs. However, we reveal that the T cells expressing transgenic TCR show more calcium activities than polyclonal T cells.

Interestingly, the antigen-specific TCR-transgenic T cells do not show elevated calcium signaling in ileal PPs. This might be due to the differences in antigen sampling machinery and tissue-specific APCs. In the PPs, the predominant APCs are M cells that uptake antigen and bacteria from the intestinal lumen (43). However, M cells are not exclusively residing in the epithelium overlaying the PPs. A different type of M cells, so-called villous M cells, can also be found in the tip of microvilli (44, 45). Furthermore, in the ileal LP, luminal microorganisms can be directly sampled via transepithelial dendrites (TEDs) of CX_3CR1^+ mononuclear phagocytes (43). Additionally, goblet cell-associated antigen passages (GAPs) can transfer luminal soluble antigens to the LP. Both TEDs and GAPs are not found in PPs but seem to be a characteristic feature of the LP (43). Those differences in antigen-sampling potentially account for the variations in the T cell calcium signaling observed in the ileal compartments. With our protocol, we do not find transferred T cells in the colon, which is different from the findings of Duc et al (46). This can be explained by the fact that we used resting nondifferentiated T cells, whereas they used activated and Th17 differentiated T cells. Another interesting organ is the mesenteric LNs (mLN) since lymphatic fluid from the small intestine passes through. Indeed, Sano et al. showed an accumulation of Th17 cells in the mLN (47). However, we do not observe elevated calcium signaling in MOG-specific T cells in mLN (16), suggesting a calcium-independent IL-17 induction in this organ, such as induction by serum amyloid A proteins as described by Sano et al (47).

To understand whether the observed calcium signaling induces transcriptional changes in the T cells, we collected the T cells from the gut-emigrating lymphatic fluid and subjected them to transcriptome analysis. GALT-emigrating T cells were compared to the T cells in the spleen. We found that the GALT-emigrating T cells from MOG TCR–transgenic mice up-regulated genes related to the Th17 axis, including *Il23R*, *Il17RE*, and *Il-22*, and activation/migration genes, such as *Shcbp1* (48), *Gabrd* (49), as well as the fibronectins

Lrfn1 and *Fndc7* (22). In line with this, Berer et al showed an increased number of IL-17, but not IFNγ, producing T cells in the ileal LP of SPF-housed mice compared to GF mice (3).

The enhanced migration of $CD4^+$ T cells was also confirmed by composition analysis of the lymphatic fluid (Fig. 7 *A* and *B*). More directly, we show the migration of MOG-specific $CD4^+$ T cells from the small intestine to the CNS in presymptomatic mice (Fig. 7*C*). Similarly, Brea et al. showed migration of pan-abT cells from the small intestine to the CNS in naive mice (50). Once the autoreactive T cells reach the CNS, they can be activated by local APCs which present endogenous antigen and subsequently produce inflammatory cytokines, which open the BBB and enhance local inflammation (6, 9). Therefore, a small number of autoreactive T cells can be enough to initiate CNS inflammation.

In conclusion, our work provides direct intravital footage of MOG-specific and other antigen-specific T cell stimulation in the ileal LP. We bring direct evidence to confirm the pivotal role of microbiota in T cell stimulation and highlight the important role of MHC class II. Moreover, we associate long-term calcium signaling with Th17-like transcriptomic changes, providing a proof-of-concept of how the MOG-specific T cells acquire their ability to trigger CNS inflammation in peripheral tissue (51). These findings also corroborate previous studies that identified the ileal LP as the site of Th17 cell induction (52, 53) and provide insights into the features and activities of autoantigen-specific T cells in the ileal LP.

Data, Materials, and Software Availability. The RNAseq data have been deposited in the Sequence Read Archive (SRA, https://www.ncbi.nlm.nih.gov/sra) (54). Accession numbers are SAMN35818795 (55), SAMN35818796 (56), and SAMN35818797 (57).

ACKNOWLEDGMENTS. We thank the Biomedical Center (BMC) Core Facility Bioimaging and the BMC Core Facility Flow Cytometry of the Ludwig-Maximilians-Universität (LMU) Munich for providing equipment, to Prof. Dirk Haller, Nutrition and Immunology, Institute for Food & Health, Technical University of Munich for providing germfree mice and Drs. Anneli Peters and Simone Mader for comments on the manuscript. This work was supported by the Deutsche Forschungsgemeinschaft (German Research Foundation) under the following projects: To N.K., research grant KA2951/2-2 (246754395), Heisenberg Programme KA2951/3-1 and KA2951/3-2 (264119140) and TRR 128 Project B10 (213904703); to D.B., Emmy Noether Programme BA5132/1-2 (252623821), SFB 1054 Project B12 (210592381), and Germany's Excellence Strategy EXC2151 (390873048); and to T.K., SFB1054 (210592381), TRR128 (213904703), TRR274 (408885537), TRR355 (490846870), and EXC 2145 (SyNergy, 390857198). In addition, T.K. is supported by the Hertie Network of Clinical Neuroscience. H.Y. and H.W. are supported by funds from Max-Planck Society. Portions of the paper were developed from the theses of I.J.B. and P.F.

Author affiliations: [a]Institute of Clinical Neuroimmunology, University Hospital, LMU Munich and Biomedical Center, Faculty of Medicine, Planegg-Martinsried 82152, Germany; [b]Institute for Experimental Neuroimmunology, Technical University of Munich School of Medicine, Munich 81675, Germany; [c]Institute for Immunology, Biomedical Center, Faculty of Medicine, Ludwig-Maximilians-Universität München, Planegg-Martinsried 82152, Germany; [d]Medical Clinic III for Oncology, Hematology, Immuno-Oncology and Rheumatology, University Hospital Bonn, University of Bonn, Bonn 53127, Germany; [e]Neuroimmunology group, Max Planck Institute of Neurobiology, Planegg-Martinsried 82152, Germany; and [f]Munich Cluster for Systems Neurology, Munich 81377, Germany

1. M. Pette *et al.*, Myelin basic protein-specific T lymphocyte lines from MS patients and healthy individuals. *Neurology* **40**, 1770–1776 (1990).
2. iMSMSConsortium, Gut microbiome of multiple sclerosis patients and paired household healthy controls reveal associations with disease risk and course. *Cell* **185**, 3467–3486.e3416 (2022).
3. K. Berer *et al.*, Commensal microbiota and myelin autoantigen cooperate to trigger autoimmune demyelination. *Nature* **479**, 538–541 (2011).
4. K. Berer *et al.*, Gut microbiota from multiple sclerosis patients enables spontaneous autoimmune encephalomyelitis in mice. *Proc. Natl. Acad. Sci. U.S.A.* **114**, 10719–10724 (2017).
5. E. Cekanaviciute *et al.*, Gut bacteria from multiple sclerosis patients modulate human T cells and exacerbate symptoms in mouse models. *Proc. Natl. Acad. Sci. U.S.A.* **114**, 10713–10718 (2017).
6. I. Bartholomäus *et al.*, Effector T cell interactions with meningeal vascular structures in nascent autoimmune CNS lesions. *Nature* **462**, 94–98 (2009).
7. D. Lodygin *et al.*, A combination of fluorescent NFAT and H2B sensors uncovers dynamics of T cell activation in real time during CNS autoimmunity. *Nat. Med.* **19**, 784–790 (2013).
8. M. Pesic *et al.*, 2-photon imaging of phagocyte-mediated T cell activation in the CNS. *J. Clin. Invest.* **123**, 1192–1201 (2013).
9. N. I. Kyratsous *et al.*, Visualizing context-dependent calcium signaling in encephalitogenic T cells in vivo by two-photon microscopy. *Proc. Natl. Acad. Sci. U.S.A.* **114**, E6381–E6389 (2017).
10. E. Bettelli *et al.*, Myelin oligodendrocyte glycoprotein-specific T cell receptor transgenic mice develop spontaneous autoimmune optic neuritis. *J. Exp. Med.* **197**, 1073–1081 (2003).
11. M. J. Barnden, J. Allison, W. R. Heath, F. R. Carbone, Defective TCR expression in transgenic mice constructed using cDNA-based α- and ß-chain genes under the control of heterologous regulatory elements. *Immunol. Cell Biol.* **76**, 34–40 (1998).
12. A. Oxenius, M. F. Bachmann, R. M. Zinkernagel, H. Hengartner, Virus-specific MHC-class II-restricted TCR-transgenic mice: Effects on humoral and cellular immune responses after viral infection. *Eur. J. Immunol.* **28**, 390–400 (1998).
13. A. H. Pham, J. M. McCaffery, D. C. Chan, Mouse lines with photo-activatable mitochondria to study mitochondrial dynamics. *Genesis* **50**, 833–843 (2012).
14. P. P. Lee *et al.*, A critical role for Dnmt1 and DNA methylation in T cell development, function and survival. *Immunity* **15**, 763–774 (2001).
15. T. Litzenburger *et al.*, B lymphocytes producing demyelinating autoantibodies: Development and function in gene-targeted transgenic mice. *J. Exp. Med.* **188**, 169–180 (1998).
16. M. Hiltensperger *et al.*, Skin and gut imprinted helper T cell subsets exhibit distinct functional phenotypes in central nervous system autoimmunity. *Nat. Immunol.* **22**, 880–892 (2021).
17. I. J. Bauer, "Visualization and functional characterization of CD4+ T cell stimulation in the ileal lamina propria", PhD Dissertation, LMU Munich (2021).
18. D. Druzd *et al.*, Lymphocyte circadian clocks control lymph node trafficking and adaptive immune responses. *Immunity* **46**, 120–132 (2017).
19. D. Kim, J. M. Paggi, C. Park, C. Bennett, S. L. Salzberg, Graph-based genome alignment and genotyping with HISAT2 and HISAT-genotype. *Nat. Biotechnol.* **37**, 907–915 (2019).
20. M. I. Love, W. Huber, S. Anders, Moderated estimation of fold change and dispersion for RNA-seq data with DESeq2. *Genome Biol.* **15**, 550 (2014).
21. A. Reboldi *et al.*, C-C chemokine receptor 6-regulated entry of TH-17 cells into the CNS through the choroid plexus is required for the initiation of EAE. *Nat. Immunol.* **10**, 514–523 (2009).
22. W. Wagner *et al.*, Adhesion of hematopoietic progenitor cells to human mesenchymal stem cells as a model for cell-cell interaction. *Exp. Hematol.* **35**, 314–325 (2007).
23. I. I. Ivanov *et al.*, Specific microbiota direct the differentiation of IL-17-producing T-helper cells in the mucosa of the small intestine. *Cell Host Microbe* **4**, 337–349 (2008).
24. V. Gaboriau-Routhiau *et al.*, The key role of segmented filamentous bacteria in the coordinated maturation of gut helper T cell responses. *Immunity* **31**, 677–689 (2009).
25. I. Cosorich *et al.*, High frequency of intestinal T(H)17 cells correlates with microbiota alterations and disease activity in multiple sclerosis. *Sci. Adv.* **3**, e1700492 (2017).
26. C. Blaschitz, M. Raffatellu, Th17 cytokines and the gut mucosal barrier. *J. Clin. Immunol.* **30**, 196–203 (2010).
27. N. Hernández-Santos, Th17 cells in immunity to candida albicans. *Cell Host Microbe* **11**, 425–435 (2012).
28. C. T. Weaver, C. O. Elson, L. A. Fouser, J. K. Kolls, The Th17 pathway and inflammatory diseases of the intestines, lungs, and skin. *Annu. Rev. Pathol.* **8**, 477–512 (2013).
29. K. Yasuda, Y. Takeuchi, K. Hirota, The pathogenicity of Th17 cells in autoimmune diseases. *Semin. Immunopathol.* **41**, 283–297 (2019).
30. T. Korn, A. C. Anderson, E. Bettelli, M. Oukka, The dynamics of effector T cells and Foxp3 + regulatory T cells in the promotion and regulation of autoimmune encephalomyelitis. *J. Neuroimmunol.* **191**, 51–60 (2007).
31. I. I. Ivanov *et al.*, Induction of intestinal Th17 cells by segmented filamentous bacteria. *Cell* **139**, 485–498 (2009).
32. Y. K. Lee, J. S. Menezes, Y. Umesaki, S. K. Mazmanian, Proinflammatory T-cell responses to gut microbiota promote experimental autoimmune encephalomyelitis. *Proc. Natl. Acad. Sci. U.S.A.* **108**, 4615–4622 (2010).
33. Y. Yang *et al.*, Focused specificity of intestinal TH17 cells towards commensal bacterial antigens. *Nature* **510**, 152–156 (2014).
34. A. Schnell *et al.*, Stem-like intestinal Th17 cells give rise to pathogenic effector T cells during autoimmunity. *Cell* **184**, 6281–6298.e6223 (2021).
35. P. Revy, M. Sospedra, B. Barbour, A. Trautmann, Functional antigen-independent synapses formed between T cells and dendritic cells. *Nat. Immunol.* **2**, 925–931 (2001).
36. A. Flügel *et al.*, Migratory activity and functional changes of green fluorescent effector T cells before and during experimental autoimmune encephalomyelitis. *Immunity* **14**, 547–560 (2001).
37. M. Pagany *et al.*, Myelin oligodendrocyte glycoprotein is expressed in the peripheral nervous system of rodents and primates. *Neurosci. Lett.* **350**, 165–168 (2003).
38. J. M. Gardner *et al.*, Deletional tolerance mediated by extrathymic Aire-expressing cells. *Science* **321**, 843–847 (2008).
39. G. Krishnamoorthy *et al.*, Myelin specific T cells also recognize neuronal autoantigen in a transgenic mouse model of multiple sclerosis. *Nat. Med.* **15**, 626–632 (2009).
40. E. Miyauchi *et al.*, Gut microorganisms act together to exacerbate inflammation in spinal cords. *Nature* **585**, 102–106 (2020).
41. K. M. Rosenthal *et al.*, Low 2-dimensional CD4 T cell receptor affinity for myelin sets in motion delayed response kinetics. *PloS One* **7**, e32562 (2012).
42. S. D. Hurst, S. M. Sitterding, S. Ji, T. A. Barrett, Functional differentiation of T cells in the intestine of T cell receptor transgenic mice. *Proc. Natl. Acad. Sci. U.S.A.* **94**, 3920–3925 (1997).
43. N. Kobayashi, D. Takahashi, S. Takano, S. Kimura, K. Hase, The roles of peyer's patches and microfold cells in the gut immune system: Relevance to autoimmune diseases. *Front. Immunol.* **10** (2019).

44. M. H. Jang *et al.*, Intestinal villous M cells: An antigen entry site in the mucosal epithelium. *Proc. Natl. Acad. Sci. U.S.A.* **101**, 6110–6115 (2004).
45. J. Wang, V. Gusti, A. Saraswati, D. D. Lo, Convergent and divergent development among M cell lineages in mouse mucosal epithelium. *J. Immunol.* **187**, 5277–5285 (2011).
46. D. Duc *et al.*, Disrupting myelin-specific Th17 cell gut homing confers protection in an adoptive transfer experimental autoimmune encephalomyelitis. *Cell Rep.* **29**, 378–390.e374 (2019).
47. T. Sano *et al.*, An IL-23R/IL-22 circuit regulates epithelial serum amyloid A to promote local effector Th17 responses. *Cell* **163**, 381–393 (2015).
48. M. W. Buckley *et al.*, Unexpected phenotype of mice lacking Shcbp1, a protein induced during T cell proliferation. *PLoS One* **9**, e105576 (2014).
49. H. Bjurstöm *et al.*, GABA, a natural immunomodulator of T lymphocytes. *J. Neuroimmunol.* **205**, 44–50 (2008).
50. D. Brea *et al.*, Stroke affects intestinal immune cell trafficking to the central nervous system. *Brain Behav. Immun.* **96**, 295–302 (2021).
51. P. Fang, "Visualizing the stimulation of encephalitogenic T cells in gut associated lymphoid tissue as a trigger of autoimmunity", PhD Dissertation, LMU Munich (2018).
52. E. Esplugues *et al.*, Control of T H 17 cells occurs in the small intestine. *Nature* **475**, 414–418 (2011).
53. A. M. Farkas *et al.*, Induction of Th17 cells by segmented filamentous bacteria in the murine intestine. *J. Immunol. Methods* **421**, 104–111 (2015).
54. N. Kawakami, Transcriptome analysis of CD4+ T cells emigrating from gut. Sequence Read Archive (SRA). https://www.ncbi.nlm.nih.gov/bioproject/986071. Deposited 21 June 2023.
55. N. Kawakami, SAMN35818795/ Transcriptome analysis of CD4+ T cells emigrating from gut. Sequence Read Archive (SRA). https://www.ncbi.nlm.nih.gov/sra/?term=SAMN35818795. Accessed 21 June 2023.
56. N. Kawakami, SAMN35818796/ Transcriptome analysis of CD4+ T cells emigrating from gut. Sequence Read Archive (SRA). https://www.ncbi.nlm.nih.gov/sra/?term=SAMN35818796. Accessed 21 June 2023.
57. N. Kawakami, SAMN35818797/ Transcriptome analysis of CD4+ T cells emigrating from gut. Sequence Read Archive (SRA). https://www.ncbi.nlm.nih.gov/sra/?term=SAMN35818797. Accessed 21 June 2023.